Mon. Not. R. Astron. Soc. **358,** 181–187 (2005) doi:10.1111/j.1365-2966.2005.08774.x

The interaction of cosmic rays and magnetized plasma

A. R. Bell★
Blackett Laboratory, Imperial College, London SW7 2AZ

Accepted 2004 December 22. Received 2004 December 22; in original form 2004 October 25

ABSTRACT

A large flux of cosmic rays streaming through a magnetized plasma creates cavities of low plasma density and low magnetic field. The magnetic field focuses the cosmic ray trajectories into the cavities with the possible formation of filaments or beams of high-energy cosmic rays.

Key words: acceleration of particles – magnetic fields – plasmas – turbulence – cosmic rays.

1 INTRODUCTION

In Paper I (Bell 2004), building on earlier work by Lucek & Bell (2000), it was shown that large fluxes of cosmic rays (CRs) can amplify a magnetic field to many times its seed value as indicated by recent X-ray observations (Vink & Laming 2003; Völk, Berezhko & Ksenofontov 2005; Yamazaki et al. 2004). Paper I considered field amplification in the context of diffusive shock acceleration of CRs at the outer shock of supernova remnants (SNRs). CR in the shock precursor drift relative to the background magnetized thermal plasma at a velocity equal to the shock velocity v_s. The CRs, assumed to consist of protons, carry an electric current $\boldsymbol{j}$ ($\boldsymbol{j}$ was called $\boldsymbol{j}_{\rm cr}$ in Paper I), which has to be approximately balanced by an oppositely directed return current $\boldsymbol{j}_{\rm return}$ carried by the thermal plasma to maintain quasi-neutrality. In the three-dimensional turbulence upstream of the shock, the two currents need not balance locally at every point in space, and the difference between the two currents is given by $\boldsymbol{j}_{\rm return} = -\boldsymbol{j} + \nabla \wedge \boldsymbol{B}/\mu_0$. The background plasma is subject to a $\boldsymbol{j}_{\rm return} \wedge \boldsymbol{B}$ force, which must be included in its momentum equation. The magnetohydrodynamics (MHD) equations for the thermal plasma are then

$$\begin{aligned} \rho\frac{{\rm d}\boldsymbol{u}}{{\rm d}t} &= -\boldsymbol{B}\wedge(\nabla\wedge\boldsymbol{B})/\mu_0 - \boldsymbol{j}\wedge\boldsymbol{B} - \nabla P,\\ \frac{\partial\boldsymbol{B}}{\partial t} &= \nabla\wedge(\boldsymbol{u}\wedge\boldsymbol{B}),\\ \frac{\partial\rho}{\partial t} &= -\nabla\cdot(\rho\boldsymbol{u}), \end{aligned} \qquad (1)$$

where P is the plasma pressure. The adiabatic equation of state, $P \propto \rho^{5/3}$, can be used to calculate P, although shock heating must be included to model the non-linear development of the interaction between the CRs and the thermal plasma. Because the CRs have a positive charge density, the thermal plasma must be negatively charged and is subject to an electric force; however, this is negligible in the limit that the speed of light is large compared with bulk plasma velocities. The electric force, due to the electric field $\boldsymbol{E} = -\boldsymbol{u}\wedge\boldsymbol{B}$, was included as the final term in equation (1) of Paper I and was shown to be small in the subsequent analysis. It was shown in Paper I that equations (1) of this paper led to an instability that is nearly purely growing when $\boldsymbol{j}$ takes the values expected in the environment of a young SNR. The linear growth rate is greatest at wavelengths ($2\pi/k$) much shorter than the CR Larmor radius $r_{\rm g}$. When $kr_{\rm g} \gg 1$, the CR trajectories are essentially unaffected by fluctuations in the magnetic field on the scale k^{-1}, and the development of the instability can be derived from equations (1) with $\boldsymbol{j}$ set equal to a value that is constant in space and time.

In Paper I, the dispersion relation was derived for the case in which $\boldsymbol{j}, \boldsymbol{k}$ and $\boldsymbol{B}_0$ are parallel, where $\boldsymbol{B}_0$ is the zeroth-order unperturbed magnetic field. The non-linear development was followed with a three-dimensional MHD code (MH3D) in which $\boldsymbol{j}$ and $\boldsymbol{B}_0$ were parallel. Three-dimensional turbulence was seen to develop and amplify the frozen-in magnetic field to a value much larger than its seed value.

In this paper, we investigate the multidimensional structure of the turbulence. The turbulence is strongly driven by the CR current $\boldsymbol{j}$. The $-\boldsymbol{j}\wedge\boldsymbol{B}$ force driving the turbulence is always perpendicular to $\boldsymbol{j}$. Consequently, the turbulence is not isotropic and its structure is different in directions parallel and perpendicular to $\boldsymbol{j}$. We present four calculations or simulations, each of which illuminates different multidimensional aspects of the turbulence, and which together give a clearer picture of the nature of the CR-driven turbulence. The first calculation is a derivation of the linear dispersion relation for general mutual orientations of CR current $\boldsymbol{j}$, zeroth-order magnetic field $\boldsymbol{B}_0$ and perturbation wavenumber $\boldsymbol{k}$, showing that most rapid growth occurs when $\boldsymbol{k}$ and $\boldsymbol{B}_0$ are parallel and that growth occurs for all orientations of $\boldsymbol{j}$ to $\boldsymbol{B}_0$. The other three calculations investigate the growth of cavities in which the magnetic field and the background plasma density become very small. A magnetic field forms around each cavity to produce magnetic forces, which focus CR trajectories into the cavity and push the thermal plasma out of the cavity. Although we are unable to self-consistently include feedback on to the CR trajectories, the focusing of CR trajectories into the cavities is sufficient to imply the eventual formation of extended filaments or beams of CR propagating through low-density cavities. The growth of filaments saturates when the electric current in filaments reaches the Alfvén current. Hence, lower limits can be estimated for the power carried by each filament or beam and for the characteristic radius of filaments or beams.

★E-mail: t.bell@imperial.ac.uk

2 LINEAR AND NON-LINEAR GROWTH OF CR-DRIVEN TURBULENCE

2.1 Linear dispersion relation

In this section the linear dispersion relation is derived for arbitrary orientation of $\boldsymbol{k}$, $\boldsymbol{B}_0$ and $\boldsymbol{j}$ showing that growth is most rapid when $\boldsymbol{k}$ and $\boldsymbol{B}_0$ are parallel, and that growth is possible at all orientations apart from $\boldsymbol{k}\cdot\boldsymbol{B}_0=0$. Although CRs tend to spiral along magnetic field lines, $\boldsymbol{j}$ and $\boldsymbol{B}_0$ can be non-parallel because of diamagnetic CR drifts or because of non-uniformities in the magnetic field on scales less than the CR Larmor radius.

The dispersion relation is derived by linear solution of equations (1). The solution takes the form

$$\xi=\xi_0+\left\{\xi_1\exp[\gamma t+\mathrm{i}\,\boldsymbol{k}\cdot\,(\boldsymbol{r}-\textstyle\int\boldsymbol{u}_0\,\mathrm{d}t)]+\mathrm{c.c.}\right\},\tag{2}$$

where c.c. denotes the complex conjugate and ξ represents $\boldsymbol{B}$, ρ, $\boldsymbol{u}$ or P. $\boldsymbol{B}_1$, ρ_1, $\boldsymbol{u}_1$ and P_1 are complex, and small compared with the zeroth-order quantities.

The zeroth-order magnetic field and density are constant, but the zeroth-order velocity increases in time because the zeroth -order $-\boldsymbol{j}\wedge\boldsymbol{B}$ force is non-zero in general, giving

$$\boldsymbol{u}_0=-\frac{\boldsymbol{j}\wedge\boldsymbol{B}_0}{\rho_0}t\tag{3}$$

if $\boldsymbol{u}_0$ is zero when $t=0$. For example, $\boldsymbol{u}_0$ is time-dependent in the case of a perpendicular shock. The diamagnetic current carried by CRs produces a $-\boldsymbol{j}\wedge\boldsymbol{B}_0$ force, which decelerates the background plasma as it flows into the shock.

The growth rate γ of first-order quantities is derived by standard procedures as outlined in Appendix A. γ is a function of the three vectors $\boldsymbol{k}$, $\boldsymbol{j}$ and $\boldsymbol{B}_0$. In Paper I, the three vectors were assumed to be collinear, but any relative orientation can be considered, giving

$$\begin{aligned}&\left[\gamma^2+(\hat{\boldsymbol{k}}\cdot\hat{\boldsymbol{b}})^2k^2v_\mathrm{A}^2\right]\left[\gamma^4+\gamma^2k^2\left(v_\mathrm{A}^2+c_\mathrm{s}^2\right)+(\hat{\boldsymbol{k}}\cdot\hat{\boldsymbol{b}})^2k^4v_\mathrm{A}^2c_\mathrm{s}^2\right]\\&\quad=\gamma_0^4\left\{\gamma^2+(\hat{\boldsymbol{j}}\cdot\hat{\boldsymbol{k}})^2k^2c_\mathrm{s}^2\right.\\&\qquad\left.+\,[(\hat{\boldsymbol{k}}\cdot\hat{\boldsymbol{b}})^2+(\hat{\boldsymbol{k}}\cdot\hat{\boldsymbol{j}})^2-2(\hat{\boldsymbol{k}}\cdot\hat{\boldsymbol{j}})(\hat{\boldsymbol{b}}\cdot\hat{\boldsymbol{j}})(\hat{\boldsymbol{k}}\cdot\hat{\boldsymbol{b}})]k^2v_\mathrm{A}^2\right\}\end{aligned}\tag{4}$$

where $\gamma_0^4=(\boldsymbol{k}\cdot\boldsymbol{B}_0)^2\boldsymbol{j}^2/\rho_0^2$, v_A is the Alfvén speed $B_0/(\mu_0\rho_0)^{1/2}$, c_s is the sound speed defined by $c_\mathrm{s}^2=\partial P/\partial\rho$, and a 'hat' denotes a unit vector: $\hat{\boldsymbol{k}}=\boldsymbol{k}/|\boldsymbol{k}|$, $\hat{\boldsymbol{j}}=\boldsymbol{j}/|\boldsymbol{j}|$, $\hat{\boldsymbol{b}}=\boldsymbol{B}_0/|\boldsymbol{B}_0|$.

If all three vectors $\boldsymbol{k}$, $\boldsymbol{j}$ and $\boldsymbol{B}_0$ are collinear as in Paper I, the dispersion relation reduces to

$$\left[\gamma^2+k^2c_\mathrm{s}^2\right]\left[\left(\gamma^2+k^2v_\mathrm{A}^2\right)^2-\gamma_0^4\right]=0.\tag{5}$$

The solution $\gamma^2+k^2c_\mathrm{s}^2=0$ corresponds to oscillatory sound waves propagating parallel to $\boldsymbol{B}_0$. The solution $(\gamma^2+k^2v_\mathrm{A}^2)^2-\gamma_0^4=0$ corresponds to transverse modes. Transverse modes are oscillatory ($\gamma^2<0$) if $k^2>\gamma_0^2/v_\mathrm{A}^2$. At longer wavelengths, $k^2<\gamma_0^2/v_\mathrm{A}^2$, there is a purely growing mode with $\gamma>0$ which produces the instability. As derived in Paper I, the maximum value of k at which growth occurs is given by $kB_0/\mu_0=j$. At shorter wavelengths, the tension in the magnetic field lines $-\boldsymbol{B}\wedge(\nabla\wedge\boldsymbol{B})/\mu_0$ exceeds and stabilizes the effect of the $-\boldsymbol{j}\wedge\boldsymbol{B}$ force, which drives the instability. At much longer wavelengths, the tension in the field lines can be neglected, $k^2v_\mathrm{A}^2$ and $k^2c_\mathrm{s}^2$ can both be neglected, and the dispersion relation has solutions $\gamma^2=0$ and $\gamma^4=\gamma_0^4$ for any mutual orientation of $\boldsymbol{k}$, $\boldsymbol{j}$ and $\boldsymbol{B}_0$.

The long wavelength limit (still assuming $kr_\mathrm{g}\gg1$) can be derived more directly from equations (1) by neglecting ∇P and $-\boldsymbol{B}\wedge(\nabla\wedge\boldsymbol{B})/\mu_0$, and defining $\boldsymbol{\Phi}=\boldsymbol{B}/\rho$ to obtain

$$\frac{\mathrm{d}\boldsymbol{u}}{\mathrm{d}t}=-\boldsymbol{j}\wedge\boldsymbol{\Phi},\qquad\frac{\mathrm{d}\boldsymbol{\Phi}}{\mathrm{d}t}=(\boldsymbol{\Phi}\cdot\nabla)\boldsymbol{u},\tag{6}$$

which yields the dispersion relation $\gamma^4=\gamma_0^4$ as above. In the purely growing solution, $\boldsymbol{u}_1$ and $\boldsymbol{\Phi}_1$ are perpendicular to each other and to $\boldsymbol{j}$, and $\boldsymbol{u}_1$ and $\boldsymbol{\Phi}_1$ rotate about $\boldsymbol{j}$ with respect to the position along the direction of $\boldsymbol{k}$. The vector $\boldsymbol{\Phi}$ has a helical structure if $\boldsymbol{k}$ is parallel to $\boldsymbol{j}$, and a sheared helical structure in general. Perturbations in $\boldsymbol{\Phi}$ ($\boldsymbol{\Phi}_1=\boldsymbol{B}_1/\rho_0-\boldsymbol{B}_0\,\rho_1/\rho_0^2$) consist of a combination of perturbations in $\boldsymbol{B}$ and ρ, depending on the mutual orientation of $\boldsymbol{k}$, $\boldsymbol{j}$ and $\boldsymbol{B}_0$. The perturbed magnetic field is given by $\boldsymbol{B}_1=\rho_0\,\boldsymbol{\Phi}_1+\mathrm{i}\gamma^{-2}\,\boldsymbol{B}_0\,(\boldsymbol{k}\wedge\boldsymbol{j})\cdot\boldsymbol{\Phi}_1$.

The dispersion relation indicates that instability is possible for all orientations of $\boldsymbol{k}$, $\boldsymbol{j}$ and $\boldsymbol{B}_0$ except for $\boldsymbol{k}$ perpendicular to $\boldsymbol{B}_0$. The growth rate of the instability is determined by the parameter $\gamma_0=(|\boldsymbol{k}\cdot\boldsymbol{B}_0|\,|\,\boldsymbol{j}|/\rho_0)^{1/2}$. The instability is strongest when the wavenumber $\boldsymbol{k}$ is parallel to the zeroth-order magnetic field $\boldsymbol{B}_0$.

2.2 A filamentary mode

In Section 2.1 the linear dispersion relation for planar modes was derived. In this section, we solve equations (1) in cylindrical (r,θ,z) geometry for the radial expansion with velocity u of a cylindrical filament. The filamentary solution gives more insight than the planar mode solution because it is closer to the natural non-linear form of the turbulence as found below in non-linear simulations.

We consider the case in which $\boldsymbol{j}$ and $\boldsymbol{B}_0$ are aligned in the z-direction and in which B_z, B_θ, u, ρ and P are functions of r alone. The twist in z of the magnetic field $k_B\,(r)=B_\theta/rB_z$ takes the place of k in the planar calculation, with a field line at radius r spiralling around the $r=0$ axis in a distance $2\pi/k_B$. Individual magnetic field lines have a helical structure, as also found in the planar calculation in Section 2.1.

In cylindrical geometry with dependence only on r and t, equations (1) take the form

$$\begin{aligned}&\frac{\mathrm{d}}{\mathrm{d}t}\left(\frac{B_z}{\rho}\right)=0,\\&\frac{\mathrm{d}}{\mathrm{d}t}\left(\frac{B_\theta}{\rho}\right)=\frac{u}{r}\left(\frac{B_\theta}{\rho}\right)\\&\frac{\mathrm{d}\rho}{\mathrm{d}t}=-\frac{\rho}{r}\frac{\partial(ru)}{\partial r}\\&\rho\frac{\mathrm{d}u}{\mathrm{d}t}=jB_\theta-\frac{\partial P}{\partial r}-\frac{B_\theta}{\mu_0 r}\frac{\partial(rB_\theta)}{\partial r}-\frac{\partial}{\partial r}\frac{B_z^2}{2\mu_0}.\end{aligned}\tag{7}$$

These equations are most easily solved by Lagrangian analysis for a fluid element at position $r(t)$ at time t and initially at position $r(0)=r_0$. The first two equations, expressing flux-freezing, give

$$\frac{B_z}{\rho}=\frac{B_{z0}}{\rho_0}\quad\text{and}\quad\frac{B_\theta}{\rho}=\frac{r}{r_0}\frac{B_{\theta0}}{\rho_0},\tag{8}$$

where B_{z0}, $B_{\theta0}$ and ρ_0 are the values of B_z, B_θ and ρ in the fluid element at time $t=0$. If the Alfvén speed v_A and the sound speed c_s are neglected as in the long wavelength approximation made for equation (6), the pressure P and the magnetic force can be neglected, and the momentum equation becomes

$$\frac{\mathrm{d}u}{\mathrm{d}t}=\frac{jB_\theta}{\rho}\quad\text{giving}\quad\frac{\mathrm{d}^2r}{\mathrm{d}t^2}=\frac{jB_{\theta0}}{r_0\rho_0}r\tag{9}$$

with the solution

$$r=r_0\exp(\gamma_0t)\quad\text{where}\quad\gamma_0=\left(\frac{jB_{\theta0}}{r_0\rho_0}\right)^{1/2}.\tag{10}$$

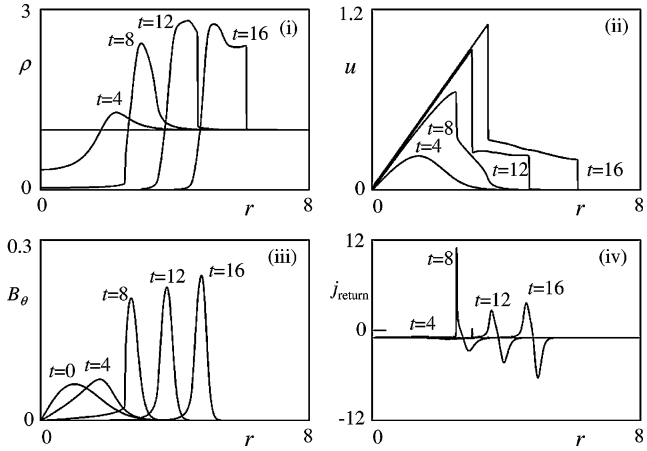

Figure 1. A filament in cylindrical geometry. Plots against radius r/r_1 at times $t/t_1 = 0$, 4, 8, 12 and 16, of (i) ρ/ρ_1, (ii) u/u_1, (iii) B_θ/B_1 and (iv) $j_{\rm return}/j$.

γ_0 is the equivalent of the same quantity in the planar analysis when kB_0 is replaced by $k_B B_{z0}(=B_{\theta 0}/r_0)$.

Filament growth is driven by the r-component (jB_θ) of the $-\boldsymbol{j} \wedge \boldsymbol{B}$ force, which accelerates the plasma away from the axis. As the plasma moves outwards, the helical field lines are extended in the θ direction, decreasing the density ρ of the plasma frozen to the field lines in the sense that $\rho \propto B_\theta/r$. The radial acceleration jB_θ/ρ consequently increases, thus increasing the expansion velocity and producing exponential growth in the radius of the helical field lines.

The solution given by equation (10) is non-linearly correct provided the pressure and magnetic forces in the thermal plasma remain negligible and as long as two adjacent fluid elements do not interchange radial positions in the analysis. As shown below, even if the pressure is initially negligible, it soon becomes important as shocks develop in the radially expanding plasma and equation (10) no longer applies.

Fig. 1 plots the expansion of a filament calculated by numerical solution of equation (7) for a uniform and constant CR current j in the z-direction. The initial filament radius is r_1, and the magnetic field is initialized with $B_z = 0.1\mu_0 j r_1$, $B_\theta = 0.1\mu_0 j r \exp(-r^2/2r_1^2)$. The $-\boldsymbol{j} \wedge \boldsymbol{B}$ force is an order of magnitude greater than the $-\boldsymbol{B} \wedge (\nabla \wedge \boldsymbol{B})/\mu_0$ pressure and tension forces due to the magnetic field, thus allowing the filament to grow. The thermal pressure is initialized with a uniform pressure $P = B_z^2/\mu_0$. In Fig. 1, ρ, u, B_θ and the return current $j_{\rm return} = [\partial(rB_\theta)/\partial r]/r\mu_0 - j$ are plotted relative to reference values ρ_1 (the initial density), $u_1 = jr_1(\mu_0/\rho_1)^{1/2}$, $B_1 = \mu_0 j r_1$ and the CR current j, respectively. The unit of distance is r_1, and the unit of time is $t_1 = r_1/u_1$.

Fig. 1 shows that plasma is expelled radially from the filament carrying with it the frozen-in magnetic field and leaving a central region in which both the plasma density and the magnetic field are very low. For the chosen parameters, the expansion is supersonic and a shock develops in front of a snowplough driven by the $-\boldsymbol{j} \wedge \boldsymbol{B}$ force. As the filament expands, the azimuthal magnetic field compresses into a relatively thin shell.

The evolution of the magnetic field is strongly constrained by the one-dimensionality of the solution and the inability of adjacent magnetic field lines to exchange position in radius. The peak magnetic field can only increase by radial compression of the magnetic field. The total magnetic energy increases as each magnetic field line is extended, but full turbulent amplification of the magnetic field is restricted by the geometry. Magnetic forces become dynamically important in three-dimensional CR-driven turbulence, as found in Paper I, but this does not occur in this one-dimensional calculation.

Fig. 1(iv) plots the return current carried by the thermal plasma as calculated from the curl of the magnetic field $j_{\rm return} = [\partial(rB_\theta)/\partial r]/r\mu_0 - j$. Because the magnetic field is initially small, the return current nearly balances the CR current at each point in radius at $t = 0$, but this is no longer so at later times $t > 8$ when $|j_{\rm return}|$ exceeds the CR current j where the gradient in B_θ is large. This is significant for the discussion in Section 4.

2.3 Non-linear structure of the magnetic field

In Section 2.2 we presented a solution for the development of a single filament in one-dimensional cylindrical geometry. We now investigate whether filaments arise naturally in less constrained three-dimensional geometries. Paper I presented a non-linear MHD calculation of three-dimensional CR-driven turbulence. The CR current $\boldsymbol{j}$ and the initial zeroth-order magnetic field were aligned in the z-direction. $\boldsymbol{j}$ was fixed in time and uniform in space. We can re-examine the calculation presented in Paper I to see if filaments develop. Figs 2 and 3 plot a series of slices in (x, y), each at a different z, of the magnitude of the magnetic field and the density at time $t = 6$ at the end of the phase of rapid non-linear development, but before the turbulence has saturated. The parameters for the calculation and further detail, including the normalization of the dimensionless parameters, can be found in section 8 of Paper I. The calculation is the same as that for which results are shown in figs 3 and 4 of Paper I, except that the initial perturbation is not precisely the same. The density and magnetic field profiles in each slice in Figs 2 and

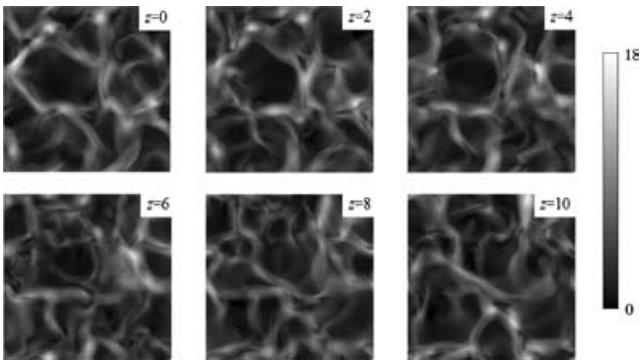

Figure 2. $|B(x, y)|$ $(0 < x < 64, 0 < y < 64)$ at $t = 6$ and $z = 0, 2, 4 \ldots 10$.

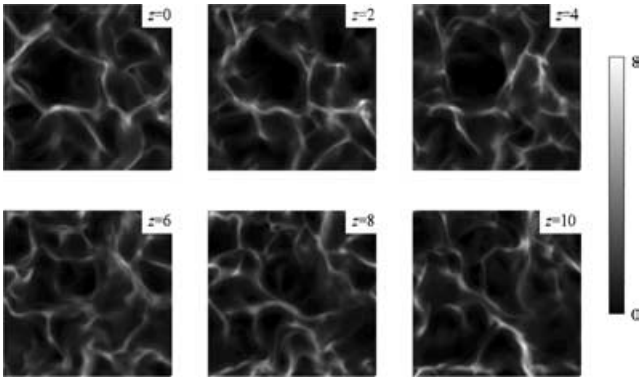

Figure 3. $\rho\ (x, y)$ $(0 < x < 64, 0 < y < 64)$ at $t = 6$ and $z = 0, 2, 4 \ldots 10$.

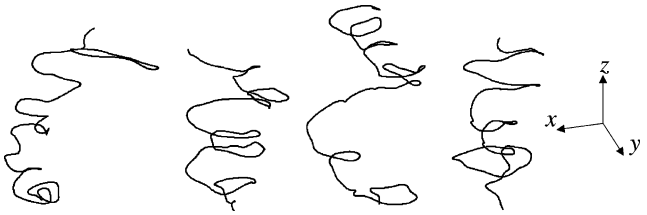

Figure 4. The paths of four magnetic field lines in (x,y,z) at $t = 6$.

3, examined individually, might be interpreted as a collection of filaments expanding into each other in (x, y). The magnetic field is concentrated in walls of strong field surrounding regions of low magnetic field and low density. The lowest density in the cavities is typically a few per cent of the initial uniform density. The component of the magnetic field perpendicular to z reverses direction across the walls of magnetic field, which is consistent with the magnetic field spiralling around the cavities with a preferred direction. This field reversal produces the dark lines in Fig. 2, representing low magnetic field, in the centre of some parts of the walls.

The plots in Figs 2 and 3 resemble slices through filaments, but comparison of nearby slices in z shows that these apparently filamentary structures are not extended in z. The length of the computational grid in x, y and z is 64 in the dimensionless units of the calculation, so the distance between each slice in z is only $1/32$ of the length of the cubic computational grid. The limited correlation between nearby slices means that the structures cannot be described as filaments. The reason for the lack of correlation in z is that there is no aspect of the physics which strongly transmits information large distances in the z-direction. CR trajectories are fixed and unaffected by the magnetic field, and hydrodynamic motions are driven predominantly perpendicular to the z-direction. However, it is energetically favourable for the instability to develop with some degree of correlation in z. Otherwise, the turbulence would consist of a series of unaligned disc-like cavities with a large magnetic shear in the (x, y) plane between adjacent discs in z and the energy in magnetic field would be large. Thus, the tension in magnetic field lines communicates some information and produces some correlation in z, but the magnetic tension is relatively weak compared with the $-\boldsymbol{j} \wedge \boldsymbol{B}$ forces driving the perpendicular motions during the early stages of the evolution of turbulence.

Although extended filaments do not develop in z, Fig. 4 shows that magnetic field lines become helical. The approximately spiral structure of field lines is consistent with the observation that the field has a preferred direction around the cavities. However, the centre of the spiral, in as much as it can be defined, wanders in the x, y plane as a field line progresses in z. The overall structure might be described as a collection of wandering filaments.

2.4 A filamentary solution driven by a CR beam

Section 2.3 has shown that, although slices in magnetic field and density at constant z resemble slices through filaments, the structures are not extended in z because no aspect of the physics strongly communicates information in the z-direction. We argue in Section 3 that this situation changes when the turbulence is fully evolved because CR trajectories are then affected by the magnetic field and transmit information along their direction of propagation. In this present section we show that, if we assume the pre-existence of a filament of intense CR flux, then a coincident low-density filament forms in the background plasma, which is accompanied by a magnetic field with the form required to further concentrate the CR trajectories into the pre-existing filament.

The three-dimensional MHD calculations presented in Section 2.3 and in section 8 of Paper I assumed that the CR current is uniform in three-dimensional space. Here, we impose a profile on the CR current

$$\boldsymbol{j}(x, y) = \boldsymbol{j}_0 \exp\left[-(x^2 + y^2)/2r_\mathrm{b}^2\right], \tag{11}$$

where $r_\mathrm{b} = 16$ is the radius of the beam in the dimensionless units of the calculation. $\boldsymbol{j}_0$ is equal to the uniform current density used in the calculations in Section 2.3. Apart from the shaping of the CR current, all aspects of the calculation, including the initial conditions, are the same as the calculation discussed in Section 2.3. Time sequences of the evolution of magnetic field and density are plotted in Figs 5(i)–(viii). Each plot is a slice in (x, y) at the same z. Initially, density and magnetic field structures grow on a scale smaller than r_b. By $t = 6$, the structures have self-organized into a filament as the dominant scalelength increases to r_b. By this time, the structure resembles the cylindrical solution found in Section 2.2, showing that this is a natural outcome for turbulence driven by a CR beam. Figs 5(ix)–(xii) plot, as a function of x and z, the mean magnetic field magnitude (averaged in y over the length L, $L = 64$, of the computational grid) $\langle|\boldsymbol{B}(x, z)|\rangle_y = \int_0^L |\boldsymbol{B}(x, z)|\mathrm{d}y/L$. At early times, a small-scale magnetic field grows within the beam. By $t = 6$, limb-brightening is consistent with the growth of a ring of magnetic field spiralling around an empty cavity. As expected, the structure is extended in z, unlike those in Section 2.3.

The evolution into a single filamentary cavity or beam might take place by a number of processes, but, whatever the details of the process, it is clear from the following general considerations that an azimuthal field must develop around the CR beam. The only way energy can be extracted from the CR beam is through an electric field E_z in the z-direction. $-jE_z$ is the rate per unit volume at which energy is given to turbulence and to the background plasma. Hence, the characteristic electric field within the beam is

$$E_z = -\frac{1}{j}\frac{\partial U_\mathrm{turb}}{\partial t} \tag{12}$$

where U_turb is the turbulent energy density. Because the electric field outside the CR beam is zero, the electric field has a non-zero curl, which gives rise to an azimuthal magnetic field

$$\frac{\partial B_\theta}{\partial t} \sim -\frac{E_z}{r_\mathrm{b}} \sim \frac{1}{jr_\mathrm{b}}\frac{\partial U_\mathrm{turb}}{\partial t} \quad \text{giving} \quad B_\theta \sim \frac{U_\mathrm{turb}}{jr_\mathrm{b}}. \tag{13}$$

The direction of E_z, and consequently B_θ, is set by the need for the electric field to decelerate the CR. The direction of B_θ is always that which results in CR beam-focusing and corresponding expulsion of plasma from the beam. This is an example of a more general phenomenon: if a charged particle beam is slowed by an electric field, then a magnetic field evolves which focuses the beam. Another example is the self-focusing of energetic laser-produced electrons propagating through a dense plasma (Bell & Kingham 2003).

The electric field in the z-direction can be calculated by an alternative method when the turbulence is still of small amplitude and can be treated as a collection of linearly growing modes with growth rates γ. Taking the simple case when the $-\boldsymbol{B} \wedge (\nabla \wedge \boldsymbol{B})/\mu_0$ force and the pressure force ∇P can be neglected so that $\rho \mathrm{d}\boldsymbol{u}_1/\mathrm{d}t = \rho\gamma\boldsymbol{u}_1 = -\boldsymbol{j} \wedge \boldsymbol{B}_1$, the second-order electric field $\boldsymbol{E}_2 = -\boldsymbol{u}_1 \wedge \boldsymbol{B}_1 = (\boldsymbol{j} \wedge \boldsymbol{B}_1) \wedge \boldsymbol{B}_1/\rho\gamma$ extracts energy from the CR beam at a rate

$$-\boldsymbol{j} \cdot \boldsymbol{E}_2 = \frac{j^2 B_\perp^2}{\gamma\rho} \tag{14}$$

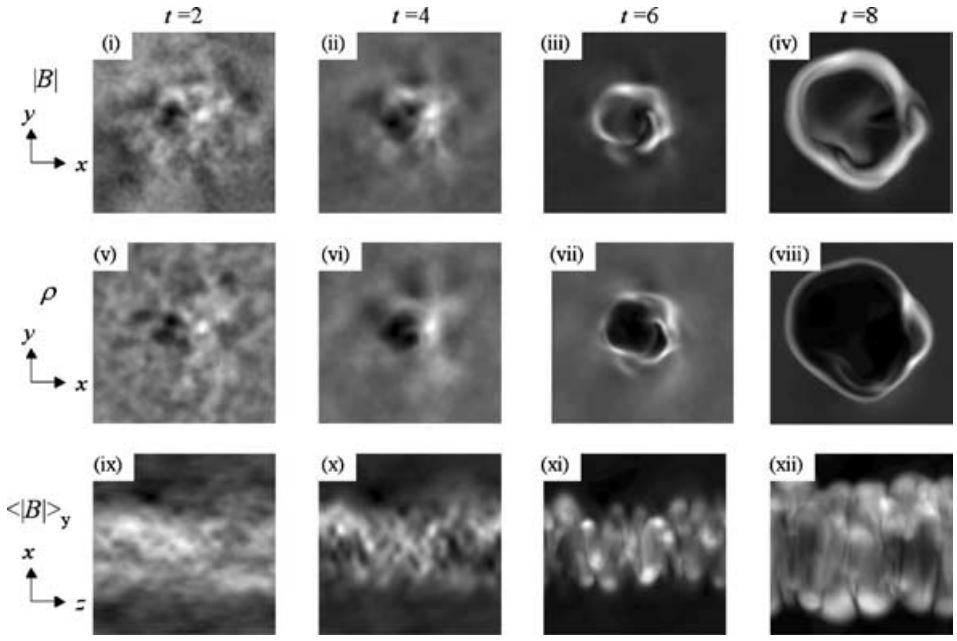

Figure 5. Turbulence driven by a beam of CRs. The plots are of $|B(x, y)|$, $\rho(x, y)$ and $\langle|\boldsymbol{B}(x, z)|\rangle_y$ in the top, middle and bottom rows, respectively. The plots are at times $t = 2$, 4, 6 and 8 in the first, second, third and fourth columns, respectively. The grey-scale minima (black) and maxima (white) for each plot as bracketed pairs (minimum, maximum) are: (i) (0.77, 1.29); (ii) (0.49, 1.89); (iii) (0.05, 5.59); (iv) (0.06, 8.83); (v) (0.78, 1.24); (vi) (0.56, 1.62); (vii) (0.14, 2.62); (viii) (0.01, 5.99); (ix) (0.95, 1.09); (x) (0.93, 1.25); (xi) (0.89, 2.58); (xii) (0.89, 3.90).

where $B_\perp$ is the component of B_1 perpendicular to j. Energy is extracted from the beam, and the CR trajectories are focused into the beam provided the turbulence is growing in amplitude ($\gamma > 0$). Equation (14) can be reconciled with equation (12) by inserting the growth rate $\gamma = (\boldsymbol{k} \cdot \boldsymbol{B}_0 j/\rho)^{1/2}$ and recognizing that the kinetic energy $\rho u_1^2/2$ exceeds the magnetic energy for wavelengths at which the magnetic tension can be neglected.

3 EVOLUTION OF TURBULENCE WHEN j AND B_0 ARE PARALLEL

In this section, we bring together the insights from Section 2 to form an overview of the evolution of turbulence through the linear phase to fully developed non-linearity. Because CRs tend to stream along the magnetic field, and differential fluid motion in the direction of $\boldsymbol{j}$ stretches the magnetic field in the same direction, $\boldsymbol{j}$ and $\boldsymbol{B}_0$ are approximately parallel in many cases. The case of parallel $\boldsymbol{j}$ and $\boldsymbol{B}_0$ is also the easiest to understand, so we confine ourselves to this case for simplicity.

Turbulence, if that is the correct word because the final state is not completely disordered, develops according to the following sequence. According to the planar mode analysis of Section 2.1, magnetic structure grows initially on scales close to $\mu_0 j/B_0$, which are much smaller than the CR Larmor radius. CR trajectories are therefore unaffected by the magnetic field perturbations. For each planar mode, the perturbed field lines form helices that grow exponentially in amplitude as the helices expand laterally. The initial small-scale perturbations non-linearly saturate at relatively small amplitudes due to tension in magnetic field lines. The dominant spatial scale becomes larger as the turbulence develops, with saturation taking place at increasing amplitude and with a magnetic field much larger than $\boldsymbol{B}_0$. As discussed in Paper I, the move to larger scales halts and the overall process saturates when the dominant scalelength becomes equal to the CR Larmor radius and the CRs gyrate around the amplified field lines. Section 2.2 gives a perspective from configuration space, which complements the Fourier space analysis of Section 2.1. Section 2.2 picks up the helical structure of the perturbed field lines found in Section 2.1 and follows in cylindrical geometry the growth of field lines close to the $r = 0$ axis and spiralling around the $r = 0$ axis. As found in the planar mode analysis the helical field lines expand laterally away from the axis, carrying with them the plasma into which they are frozen and forming a density cavity on the axis. Slices perpendicular to $\boldsymbol{j}$ (and $\boldsymbol{B}_0$) in the non-linear calculation of Section 2.3 demonstrate the development of cavities in which both the plasma density and magnetic field are very small. The size of the cavities increases with time, and this corresponds to the evolution towards large scalelengths indicated by the planar mode calculation. The cavities are formed by $-\boldsymbol{j} \wedge \boldsymbol{B}$ acceleration of the background fluid perpendicular to $\boldsymbol{j}$, and hence the cavities tend to be disc-like rather than filamentary. Tension in field lines produces some correlation in the direction of $\boldsymbol{j}$ so the overall picture of magnetic field line structure is of a collection of wandering helices. The field lines wind around the cavities with a preferred orientation which produces the $-\boldsymbol{j} \wedge \boldsymbol{B}$ force that causes the cavity to expand. The cavities initially expand exponentially in time, but non-linearly encounter nearby cavities expanding towards them, whereafter cavity expansion continues but at a slower rate. The plasma between adjacent cavities is compressed producing high-density, high magnetic field walls between cavities. The plasma in the walls is heated by compression and shocks. Because the magnetic field winds in a preferred direction about each cavity, the magnetic field changes direction within the walls.

The overall process saturates when the scalelength becomes comparable with the CR Larmor radius. In configuration space, this can be expected to correspond to the situation in which the cavity dimensions have expanded to equal the CR Larmor radius. Although

CRs are able to pass easily through the low magnetic field in the cavities, the CR current is then unable to penetrate the large magnetic field in the wall, and the $-\boldsymbol{j} \wedge \boldsymbol{B}$ force causing the cavity to expand is much reduced at this stage. The calculations of Section 2 cannot fully address the saturation phase because the feedback of magnetic field on to the CR trajectories needs to be included in the model.

In the saturation phase, CR trajectories are affected by the magnetic field. As this phase is approached, the first effect will be that each cavity acts as a lens focusing the CR trajectories. The $-\boldsymbol{j} \wedge \boldsymbol{B}$ force, which acts to expand the cavity, also reacts to deflect CR towards the centre of the cavity as required by momentum conservation. The CR trajectories are focused towards a point downstream of the cavity, thus increasing the downstream $-\boldsymbol{j} \wedge \boldsymbol{B}$ forces and creating a cavity downstream of the first cavity. The second cavity produces cavitation yet further downstream and a filament is formed. In contrast with earlier stages in the evolution of turbulence, once the CR trajectories are deflected by the turbulent magnetic field, there is now a mechanism to transfer information along the direction of $\boldsymbol{j}$ and cause the cavities to develop as filaments.

The interaction between CRs and the background plasma is analogous to the filamentation of laser light as it passes through a plasma (Kruer 1988; Young 1991). It is particularly analogous to thermal self-focusing (Craxton & McCrory 1984) in which a beam of laser light heats the plasma through which it passes. The increased thermal pressure in the beam drives thermal plasma out of the beam, creates a density cavity, and the refractive index focuses the laser light into the cavity. The feedback process between plasma heating, increased thermal pressure, cavity formation and refraction can cause a laser beam to self-focus or a uniform laser beam to break into filaments. Ideally, we would model the analogous self-consistent feedback of the magnetic field on to a CR beam to calculate whether CR self-focusing occurs, but we do not have the computational resources needed to model adequately the CR trajectories. However, Section 2.4 demonstrates that CRs focused to a higher flux by a cavity would tend to produce a downstream filament if we were able to model the CR trajectories.

The picture of turbulence developed in this section applies if the CRs are mono-energetic. Normally, CRs with a large range of energies would participate in the process producing turbulence on a large range of spatial scales and evolutionary time-scales. The interaction between turbulence on different scales is beyond the scope of this paper.

4 THE POWER IN EACH CAVITY OR FILAMENT

The turbulence saturates when the radius R of cavities, or filaments, is comparable to the CR Larmor radius, that is when $R \sim r_{\rm g} = \epsilon/cB$ where ϵ is the energy of the CRs in eV. The electric current passing through the cavity is then $I = 2\pi RB/\mu_0 \sim 2\pi\,\epsilon/c\mu_0$. This current is the Alfvén current, although the Alfvén current is often defined without the factor of 2π (Miller 1982). The Alfvén current is the maximum current that can be carried by a charged particle beam without the beam pinching under its own self-generated magnetic field. In our case, the current $I_{\rm cr}$ carried by the CR is balanced by an oppositely directed return current $I_{\rm return}$ carried by the thermal plasma, and the total current is given by the sum, $I = I_{\rm cr} + I_{\rm return}$. For the calculation in Section 2.2, Fig. 1(iv) shows that the return current within the cavity balances the CR current, $j_{\rm return} \approx -j$, but that $|j_{\rm return}|$ can be large compared to j at the edge of the cavity where the magnetic field is strong and has large gradients. We define $\chi = I/I_{\rm cr}$ as the ratio of the total current to that carried by the CRs, in which case the power carried by CRs through the cavity is

$$\mathcal{P}_{\rm cr} = I_{\rm cr}\epsilon = I\epsilon/\chi \sim 2\pi\epsilon^2/\chi c\mu_0 = 1.7 \times 10^{28}\epsilon_{15}^2/\chi \ \ {\rm W}, \qquad (15)$$

where ϵ_{15} is the CR energy in units of 10^{15} eV. Because $\chi \leqslant 1$, equation (15) gives a lower bound on the CR power through each cavity or filament at saturation. In the case of Fig. 1(iv), χ is less than one, but not by orders of magnitude. Consequently, the Alfvén current provides a good first estimate of the characteristic CR current carried by a filament.

If the energy density $U_{\rm cr}$ of high-energy CRs producing the cavity is a fraction f of $\rho v_{\rm s}^2$, where the SNR shock propagates at velocity $v_{\rm s}$ into a medium of density ρ, then $f\rho v_{\rm s}^3$ is the CR energy flux relative to the upstream plasma and $\mathcal{P}_{\rm cr} = \pi R^2 f \rho v_{\rm s}^3$. A discussion of the upstream energy density of high-energy CRs, and hence the value of f, can be found in section 7 of Paper I. Substituting the expression for $\mathcal{P}_{\rm cr}$ into equation (15) gives an estimate for the filament radius

$$R \sim \left(\frac{2\epsilon^2}{\chi c\mu_0 f \rho v_{\rm s}^3}\right)^{1/2} \sim 6 \times 10^{14}\epsilon_{15}\chi^{-1/2} f_{0.01}^{-1/2} n_{\rm cm}^{-1/2} v_7^{-3/2} \ {\rm m} \qquad (16)$$

where $n_{\rm cm}$ is the upstream nucleon density in cm^{-3}, v_7 is the shock velocity in units of 10^7 ms^{-1} and $f_{0.01} = f/0.01$.

The estimate for the filament radius in equation (16) indicates that high-energy CRs may be able to drive cavities or filaments that are large enough to be observable. However, it is questionable whether the cavities have time to self-organize into extended filaments on the large scale in SNRs. The cavities are hydrodynamic structures driven by the CR pressure, which has a magnitude $P_{\rm cr} = f\rho v_{\rm s}^2/3$, and the characteristic hydrodynamic, or acoustic, velocity $(P_{\rm cr}/\rho)^{1/2}$ associated with the CR pressure is $(f/3)^{1/2}v_{\rm s}$. In the characteristic time $R_{\rm s}/v_{\rm s}$ taken for a SNR shock to expand through the SNR radius $R_{\rm s}$, cavity or filament formation is probably unlikely on scales greater than $\sim f^{1/2}R_{\rm s}$, but further work is needed to determine whether large cavities or filaments might be expected upstream of SNR shocks. Large-scale CR filaments or beams are more likely in other objects in which CR are injected into the surrounding medium over a long period of time. In SNRs, conditions for filamentation may occur at very early stages in which the SNR shock propagates through a circumstellar wind. The circumstellar wind density decreases with radius, and a large flux of CR, produced at high density, might escape into a low-density medium, which is easily modified by the CR pressure.

5 SUMMARY

We have shown that in suitable conditions, streaming CRs interact with a background thermal plasma to create cavities of low density and low magnetic field. The non-linear development of these structures is expected to saturate when the radius of the cavity is comparable with the CR Larmor radius. The orientation of the magnetic field is such as to focus the CR trajectories into the cavity. Given sufficient time this may lead to filamentation in the CR flux. If the process reaches saturation, the power carried by CRs passing through each cavity or filament is at least $1.7 \times 10^{28}\epsilon_{15}^2$ W.

REFERENCES

Bell A. R., 2004, MNRAS, 353, 550 (Paper I)
Bell A. R., Kingham R. J., 2003, Phys. Rev. Lett., 91, 035003
Craxton R. S., McCrory R. L., 1984, J. Appl. Phys., 56, 108
Kruer W. L., 1988, The Physics of Laser–Plasma Interactions. Addison-Wesley, Reading, MA
Lucek S. G., Bell A. R., 2000, MNRAS, 314, 65
Miller R. B., 1982, An Introduction to the Physics of Intense Charged Particle Beams. Plenum, New York
Vink J., Laming J. M., 2003, ApJ, 584, 758
Völk H. J., Berezhko E. G., Ksenofontov L. T., 2005, A&A, in press (astro-ph/0409453)
Yamazaki R., Yoshida T., Terasawa T., Bamba A., Koyama K., 2004, A&A, 416, 595
Young P. E., 1991, Phys. Fluids B, 3, 2331

APPENDIX

Here we outline a derivation of the dispersion relation (equation 4). The equations to be linearized and solved are (equation 1)

$$\rho\frac{\mathrm{d}\boldsymbol{u}}{\mathrm{d}t} = -\boldsymbol{B}\wedge(\nabla\wedge\boldsymbol{B})/\mu_0 - \boldsymbol{j}\wedge\boldsymbol{B} - \nabla P,$$
$$\frac{\partial\boldsymbol{B}}{\partial t} = \nabla\wedge(\boldsymbol{u}\wedge\boldsymbol{B}),$$
$$\frac{\partial\rho}{\partial t} = -\nabla\cdot(\rho\boldsymbol{u})$$

and the solution takes the form

$$\xi = \xi_0 + \left\{\xi_1\exp[\gamma t + \mathrm{i}\,\boldsymbol{k}\cdot(\boldsymbol{r} - \int \boldsymbol{u}_0\,\mathrm{d}t)] + \text{ c.c.}\right\}$$

where 'c.c.' denotes the complex conjugate and ξ represents $\boldsymbol{B}$, ρ, $\boldsymbol{u}$ and P. $\boldsymbol{B}_1$, ρ_1, $\boldsymbol{u}_1$ and P_1 are complex and small compared with the zeroth-order quantities $\boldsymbol{B}_0$, ρ_0, $\boldsymbol{u}_0$ and P_0. If $\boldsymbol{j}$ and $\boldsymbol{B}_0$ are not parallel, the zeroth-order velocity $\boldsymbol{u}_0$ increases in time:

$$\boldsymbol{u}_0 = -\frac{\boldsymbol{j}\wedge\boldsymbol{B}_0}{\rho_0}\,t.$$

The first-order equations are

$$\gamma\rho_0\boldsymbol{u}_1 = -\boldsymbol{j}\wedge\boldsymbol{B}_1 + \boldsymbol{j}\wedge\boldsymbol{B}_0\frac{\rho_1}{\rho_0} - \frac{\mathrm{i}\boldsymbol{B}_0}{\mu_0}\wedge(\boldsymbol{k}\wedge\boldsymbol{B}_1) - \mathrm{i}\boldsymbol{k}c_\mathrm{s}^2\rho_1$$
$$\gamma\boldsymbol{B}_1 = \mathrm{i}\boldsymbol{k}\wedge(\boldsymbol{u}_1\wedge\boldsymbol{B}_0),$$
$$\gamma\rho_1 = -\mathrm{i}\rho_0(\boldsymbol{k}\cdot\boldsymbol{u}_1)$$

where $c_\mathrm{s}^2 = \partial P/\partial\rho$ is the square of the sound speed. These can be reduced to a single equation in $\boldsymbol{u}_1$

$$\begin{aligned}\gamma^2\boldsymbol{u}_1 = &-\mathrm{i}\gamma_0^2\hat{\boldsymbol{j}}\wedge\boldsymbol{u}_1 - k^2c_\mathrm{s}^2(\hat{\boldsymbol{k}}\cdot\boldsymbol{u}_1)\hat{\boldsymbol{k}} - k^2v_\mathrm{A}^2\\ &\times\left\{(\hat{\boldsymbol{k}}\cdot\hat{\boldsymbol{b}})^2\boldsymbol{u}_1 - (\hat{\boldsymbol{k}}\cdot\hat{\boldsymbol{b}})(\hat{\boldsymbol{k}}\cdot\boldsymbol{u}_1)\hat{\boldsymbol{b}}\right.\\ &\left.-(\hat{\boldsymbol{k}}\cdot\hat{\boldsymbol{b}})(\hat{\boldsymbol{b}}\cdot\boldsymbol{u}_1)\hat{\boldsymbol{k}} + (\hat{\boldsymbol{k}}\cdot\boldsymbol{u}_1)\hat{\boldsymbol{k}}\right\}\end{aligned}$$

where $\gamma_0^2 = (\boldsymbol{k}\cdot\boldsymbol{B}_0)j/\rho_0$, v_A is the Alfvén speed $B_0/(\mu_0\rho_0)^{1/2}$, and 'hat' denotes a unit vector (e.g. $\hat{\boldsymbol{b}}$ is the unit vector in the direction $\boldsymbol{B}_0$). The next step in the derivation is to set up a coordinate system with axes defined by unit vectors $\boldsymbol{i}_1$, $\boldsymbol{i}_2$ and $\boldsymbol{i}_3$ in the directions $\boldsymbol{k}$, $\boldsymbol{k}\wedge(\boldsymbol{k}\wedge\boldsymbol{B}_0)$ and $\boldsymbol{k}\wedge\boldsymbol{B}_0$. $\boldsymbol{u}_1$ and $\boldsymbol{j}$ can have non-zero components in each of the three directions. $\boldsymbol{B}_0$ can have non-zero coordinates in only the first two directions, and $\boldsymbol{k}$ is non-zero only in the first direction. Three simultaneous equations can be derived for the three components of $\boldsymbol{u}_1$. The solution for $\boldsymbol{u}_1$ is non-zero if

$$\begin{vmatrix}\gamma^2 + k^2c_\mathrm{s}^2 + (1-b_1^2)k^2v_\mathrm{A}^2 & -\mathrm{i}\gamma_0^2j_3 - b_1b_2k^2v_\mathrm{A}^2 & \mathrm{i}\gamma_0^2j_2\\ \mathrm{i}\gamma_0^2j_3 - b_1b_2k^2v_\mathrm{A}^2 & \gamma^2 + b_1^2k^2v_\mathrm{A}^2 & -\mathrm{i}\gamma_0^2j_1\\ -\mathrm{i}\gamma_0^2j_2 & \mathrm{i}\gamma_0^2j_1 & \gamma^2 + b_1^2k^2v_\mathrm{A}^2\end{vmatrix} = 0$$

where $b_1 = \boldsymbol{i}_1\cdot\hat{\boldsymbol{b}}$, $b_2 = \boldsymbol{i}_2\cdot\hat{\boldsymbol{b}}$, $j_1 = \boldsymbol{i}_1\cdot\hat{\boldsymbol{j}}$, $j_2 = \boldsymbol{i}_2\cdot\hat{\boldsymbol{j}}$, and $j_3 = \boldsymbol{i}_3\cdot\hat{\boldsymbol{j}}$ are the non-zero components of $\hat{\boldsymbol{b}}$ and $\hat{\boldsymbol{j}}$, respectively. From this, the derivation of the dispersion relation (equation 4) is straightforward.

This paper has been typeset from a TEX/LATEX file prepared by the author.